Effects of Sand and Process Water pH on Toluene Diluted Heavy Oil in Water Emulsions in Turbulent Flow

Chandra W. Angle and Hassan A. Hamza
Natural Resources Canada, CANMET Energy Technology Centre-Devon, Advanced Separation Technologies, Devon, Alberta, Canada T9A 1A8

DOI 10.1002/aic.11649
Published online November 10, 2008 in Wiley InterScience (www.interscience.wiley.com).

The presence of sand in heavy oil production is known to enhance oil recovery. Sand can also be detrimental depending on the properties of the sand–water interface. In this process, the water soluble material interacts with both sand and oil droplets and affects emulsion stability. The formation and stability of heavy oil-in-water emulsions during turbulent flow using batch process stirred-tank mixing of oil, sand, and water were investigated at three pH. Size distributions were measured by laser diffraction. High-speed video photomicrography was used to observe the process during mixing. Results showed that the presence of sand enhanced formation of stable, fine emulsion at basic pH 8.5. When the pH of the water was reduced below 6.5 both sand and droplets surface properties changed, the emulsions became less stable and coalescence was apparent. The sand grains acted as coalescers at low pH and enhanced breakage at high pH. © *Her Majesty the Queen in Right of Canada, as represented by the Minister of Natural Resources, 2008 AIChE J,* 55: 232–242, 2009
Keywords: energy, environmental engineering, interfacial processes, petroleum, mixing

Introduction

Fluids produced in heavy oil extractions are often mixed with sand during flow. Emulsions of various size distributions and stabilities are created and require treatment to separate oil from water. Our previous studies showed that at pH 8.5 in model process water, the sizes of emulsions created in the presence of sand were smaller and more stable than those created without sand.[1] We also showed that for increased fractions of sand mixed with a fixed fraction of a toluene-diluted heavy oil in fully turbulent flow (Rushton turbine in a stirred tank), the droplet breakage rate increased with increased sand fractions.[1] A first order kinetic breakage rate function described the decreasing emulsion droplet size during mixing at fixed energy dissipation for all fractions of sand present in model process water at fixed pH of 8.5. Steady-state droplet size was shown to be a function of the sand fraction for equal energy dissipation rates. The emulsion droplets remained stable over weeks and months.[1] In the absence of sand in model process water pH 8.5, the sizes and stability of toluene-diluted heavy oil droplets depended on the oil fraction as well as on the concentration of oil in toluene during turbulent mixing.[2–6]

Treating produced fluids from sandy new wells was also previously proven to be difficult because demulsifiers that were ordinarily effective became ineffective. The demulsifiers adsorbed on the coarse sand which then became wetted by oil while making oil/water separations ineffective in the produced water.[5] As well, acid treatment for a "soak" period in conditioning of wells before production causes a decrease of pH. After such conditioning, complex fluids containing oil emulsions, sand, and water that are produced must be separated. This suggested that changing water quality may also impact on the separation of emulsions from sand and water and these processes must be understood. To our knowledge

Correspondence concerning this article should be addressed to Chandra W. Angle at angle@nrcan.gc.ca.

to date, there are no published data which describe the effect of reduced pH on droplets sizes and stability behavior during turbulent mixing with and without sand. We chose three pH that represented typical dissociation equilibria in the acid titration curve of a process water.

In previous work, we used the Komolgorov's theory that discusses restorative interfacial tension forces (in the Laplace pressure equations) that counteract turbulent stresses which deform the oil droplets.[4] For the present study, we follow-up the previous studies on the properties of the heavy oil components and oil/water interfaces[2–7] by further characterization of interfaces and droplet sizes in process water of various pH. At the oil/water interface, the surface-active functional groups present may become more polar, dissociate and reorganize, and compete for space with other molecules. Water quality may affect adsorption of dissolved surfactants at the oil/water interfaces and change interfacial properties. Thus, to explain the changes in the emulsion stability observed during mixing in various waters for this work, we measured the dynamic interfacial tension at the oil/water interface as a function of time and pH of the aqueous phase, the zeta potentials of oil droplets and fine sand particles, and the emulsion size distributions. The Sauter mean diameters as a function of mixing times as well as selected microscopic images of droplets are reported to show the progressive changes.

Experimental

Materials and methods

Heavy oils from two SAGD production wells at Primrose, Alberta, Canada, were pooled. Within 24 h of arrival the fluids were separated and analyzed by Dean and Stark extraction.[8] The water-free toluene-diluted heavy oil was rotary evaporated (120°C and 8 kPa vacuum pressure) to remove all remaining solvent. The analytical properties of this heavy oil were measured and are shown in Table 1. From the solvent-free heavy oil, a 25-wt % heavy oil stock was prepared 2–3 h before being used and is referred to as the "oil" from hereon. A 25-g portion of oil and 75 g toluene were shaken in a horizontal laboratory shaker until no oil lumps were seen under the microscope at 60× magnification. The properties of the diluted oil at 22°C are shown in Table 2.

The model process water (mpH_2O) was prepared by dissolving $NaHCO_3$ (0.01 mol/l), $CaCl_2$ (1.8×10^{-6} mol/l), and K_2CO_3 (1.37×10^{-4} mol/l) in 1 l deionized water (dH_2O). The pH of the mpH_2O was 8.5 and specific conductivity (SC) was 870 μS/cm at 25°C. The pH of mpH_2O was adjusted to 8.5, 6.5, and 3.5 as needed by using Fisher ACS-grade 2 mol/l HCl and 2 mol/l NaOH.

The salts $NaHCO_3$, $CaCl_2$, K_2CO_3, and KCl were 99.99% purity Sigma-grade obtained from Aldrich Chemicals. The 2 mol/l H_2SO_4 was Fisher ACS-grade. The pH buffers (4.0, 7.0, 10.0) and conductivity standards (KCl) were preprepared Fisher Scientific Products. Spectroscopic or HPLC purity (Optima) organic solvents $CHCl_3$, CH_2Cl_2, *n*-heptane (for asphaltenes analysis), toluene, and acetone (for cleanup) were from Fisher Scientific. Food-grade 35-wt % H_2O_2 used for pretreating the sand was obtained from HCI Canada. The detailed cleaning and preparation methods of the sand were described previously.[1] Size analysis of the sand by light scattering gave a wide size distribution, d_{10} = 221 μm, d_{50} = 303 μm, d_{90} = 413 μm, d_{32} = 294 μm. The zeta potential sand was −45 mV in mpH_2O at pH 8.5.

Table 1. Properties of the Primrose Heavy Oil

API	11
Saturates	23.0 wt %
Aromatics	21.1 wt %
Resins	38.8 wt %
Asphaltenes	17.1 wt %
Molecular weight	534 g/mol[9]
Density 22°C	1003 kg/m^3
Viscosity at 24°C	>10,000 mPa s

Table 2. Properties of 25 wt% Heavy Oil in Toluene

Density	895.45 kg/m^3
Viscosity	1.56 mPa s
Interfacial tension (oil/mpH_2O)	19.9 mN/m
Resin/asphaltenes, mass ratio	2.27
Asphaltenes	4.28 wt %

Zeta potential

Zeta potentials of colloidal sand and O/W emulsions were determined by using the Brookhaven ZetaPALS (Brookhaven, New York) electrophoretic instrument. Electrophoretic mobility (EM) measurements were conducted by using palladium electrodes fitted in a glass cuvette at a fixed electric field strength that was determined after measuring the sample conductance. Using phase analysis of light scattering (PALS) of particles at fixed frequency, the EM was converted to zeta potential using Smoluchowski equation.[9,10] Details of the technique are published elsewhere.[10,11]

Interfacial tension

Dynamic interfacial tensions of the oil in the various waters were measured by the drop volume technique using a Krüss DVT-10 tensiometer, and near static interfacial tension measurements were measured after longer equilibration times using the Kruss-K12 tensiometer and the du Nouy technique.[10]

Mixing and size distribution measurements

Details of the apparatus, procedures for mixing, sampling, and analysis were previously described in other publications.[1] Figure 1 is a schematic of the apparatus used. It has a fully baffled 1-l flat-bottomed glass cylindrical tank of diameter D_T = 10.43 cm with liquid height $H = D_T$ giving a sample volume 891.7 ml, a Rushton turbine of diameter D = 5.08 cm (blades of width w = 1.02 cm, length b_{bl} = 1.24 cm are mounted equidistant around a circular disc). The off-bottom clearance was $D_T/3$. The turbine and Teflon lid were centered at the middle of the tank. All wetted surfaces in both mixing and sampling were made of stainless steel, glass, or PTFE (Teflon). The power number was 5.1 ± 0.3 for this apparatus using a Lightnin mixer-motor with digital controls for speeds up to 2000 rpm, time precise to 0.01 min, and power consumption at a precision of ±0.1 W. The mixing speed for the experiments was at 800 rpm (Re > 35,000, see notation).

Preweighed and diluted oil phase (25 wt % heavy oil in toluene) were gently poured over the surface of the water forming the oil layer that was equilibrated with the water for

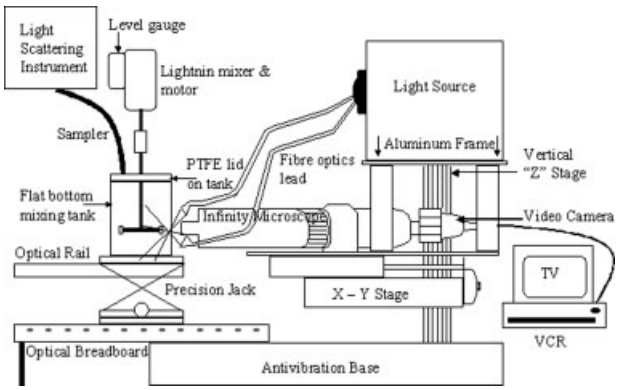

Figure 1. Schematic of the mixing and size detection apparatus.[1]

1.5 h. During the equilibration time, when the oil and water would become mutually saturated, the sampling ports of the tank were sealed and the top of the vessel was wrapped in aluminum foil to prevent evaporation.

The Mastersizer 2000 with the HydroSm sampler (Malvern, UK) and Nikon E600 microscope were readied for size analysis during equilibration of the oil and water. The carrier fluid (160 ml capacity) of the HydroSm sampler was circulated using an axial impeller at a speed of 3010 rpm for flow without additional shearing. The fluid was the same as the water in the mixing tank.

After oil/water equilibration, the Lightnin motor was adjusted to the desired speed. Mixing and timing were started simultaneously. After each prescribed time of mixing, a sample was removed for analysis. The samples were extracted with a graduated disposable Luer lock syringe of 0.4 cm orifice, fitted with a 0.45 cm diameter stainless steel needle. The needle was attached to a 0.45 cm internal diameter (i.d.) PTFE tube that was situated at the impeller offshoot level for sampling as needed. This ensured that the samples were taken where the velocity of the moving fluid was the greatest and while the whole system was in continuous turbulent flow. Sampling and measurements were done quickly to maintain the sample integrity.

When sand was present, the mixer was stopped and within less than 10 s 1 ml fluid was aspirated through the wide PTFE tube into the syringe, flow was resumed and 0.5 ml of the sample was immediately deposited into the flowing carrier fluid of the Hydrosm sampler and size distribution was measured immediately. Size measurements were made in 12 s during which the laser light scattering instrument took 12,000 snapshots of the scattering particles per aliquot. Duplicate measurements were made of the same aliquot for the specified mixing time. All data were stored on the computer for further analysis. Selected experiments were also video recorded over time of mixing [for each of the three phases (oil, sand, water) mixing experiment and at the end of the two phase (oil, water) mixing experiments].

Microscopy

Light microscopy was used alongside the light scattering technique for verification of the trends observed and for observing other visual details in the samples. Typical microscope objectives used were 40× or 60× designed for extra (ELWD) depth and field of view. The emulsion samples were examined and recorded immediately (10 s) after sampling from the mixing tank. A portion of each emulsion sample was placed into 100–500 μm deep quartz Helma microscope slides and covered with an 18-mm glass cover slip. Using a Nikon Coolpix AE950 digital camera and the Nikon E600 microscope, the droplets were photographed within 10 s of sampling. Digital files were stored in the computer. Droplet diameters were less than 100 μm in most cases. The 500-μm slides were best for the larger droplets.

The emulsification of oil was tested at one volume fraction of sand $\Phi_{sand} = 0.15$. The sand was mixed at 800 rpm with model process water (mpH_2O) at pH 8.5. The other waters used were mpH_2O at pH 8.5, 6.5, and 3.5 to reflect conditions in a "post-soak" production well start-up. Equilibrated oil volume fractions of $\Phi_{oil} = 0.05$ or 0.1 were mixed for 100 min and emulsion sampling times were 1, 8, 15, 25, 35, 45, 60, 75, 90, and 100 min during agitation. All emulsions were re-examined after 24 h rest, then selectively after 48 h or longer. Controls consisted of the samples measured without sand but otherwise under identical mixing conditions. The Reynolds number *Re* was 35,000 indicating that flow was fully turbulent for all runs. Weber numbers *We* were 1169 at pH 8.5, 994 at pH 6.5, and 984 at pH 3.5.

Results and Discussion

From Hinze-Kolmogorov theory, interfacial tension plays a major role in droplet breakup in dilute model systems during turbulent flow.[12,13] It has also been established by the theory of stability of lyophobic colloids that the sum of the van der Waals attractive forces and electrical double layer repulsive forces are key factors influencing droplet–droplet coalescence behavior in relatively static systems.[14] The total potential energy V_T is the sum of competing contributions from the long range forces V_A attractive, V_R repulsive and the short-range hydration forces V_S (usually a small contribution that works only from a few nanometers between bodies).

$$V_T = V_A + V_R + V_S \tag{1}$$

$$V_A = -A/(12\pi H^2) \tag{2}$$

where A is the Hamaker constant and H is the interparticle separation.

$$V_R = 2\pi\varepsilon a\varsigma^2 \exp(-\kappa H) \tag{3}$$

where a is the particle radius, κ is the inverse electrical double layer thickness dependent on the ionic strength, and ζ is the zeta potential. V_A is small relative to V_R for charged colliding droplets (in Brownian motion or during agitation). V_A is a function of the $1/H^2$. V_R is a function of ζ^2. After the repulsive energy barrier is overcome, the particles attraction (described in the primary minimum of the total energy curve) pulls particles together irreversibly to promote coalescence, which is a complex and irreversible process. For particles that are close enough to flocculate, in a secondary minimum of the total energy curve (larger H), the flocs may be easily broken up by agitation.

Experimentally the significant change in the droplets surface properties brought about the change to the repulsive forces via the changes in the zeta potential. Thus we will not elaborate on the V_A. The measured zeta potential indicates the magnitude of repulsive forces between the droplets, if we neglect hydration forces V_S.

For this article, the dynamic and near static interfacial tensions, as well as the zeta potentials as a function of pH, are presented first to indicate the surface properties and stability of the droplets. Next, the emulsion formation kinetics in turbulent flow as a function of pH of mpH_2O in the presence of sand is compared without sand. The pH referred to in this study is generally the initial pH of the water. Droplet stability decreased as pH decreased below 8.5.

Dynamic interfacial tension of oil in mpH_2O at three pH

IFT-time behaviors of heavy oil in mpH_2O at pH 8.5, 6.5, and 3.5 are shown in Figures 2 and 3. Figure 2 shows the dynamic interfacial tension σ_{dyn} measured by the drop volume technique (DVT) plotted against time (heavy-oil droplet age in seconds) for pH 8.5, 6.5, and 3.5. The σ_{dyn} vs. time curve at pH 8.5 shows the highest interfacial activity indicated by lowest interfacial tension values and a steeper interfacial tension gradient with droplet age in comparison with those for pH 6.5 and 3.5. The sharp decrease in dynamic interfacial tension for a drop age of seconds would indicate either an initial rapid adsorption at the interface or fast interface reaction kinetics of material that enhance surface activity. The uppermost curve is for pH 3.5 and shows the largest σ_{dyn} vs. time. Interfacial tensions for droplets aged in water at pH 6.5 are between those for pH 3.5 and 8.5. As the pH is lowered and interfacial tension became higher, perhaps transport of surface active species to the interface or dissociation of surface functional groups is lessened. An increased time

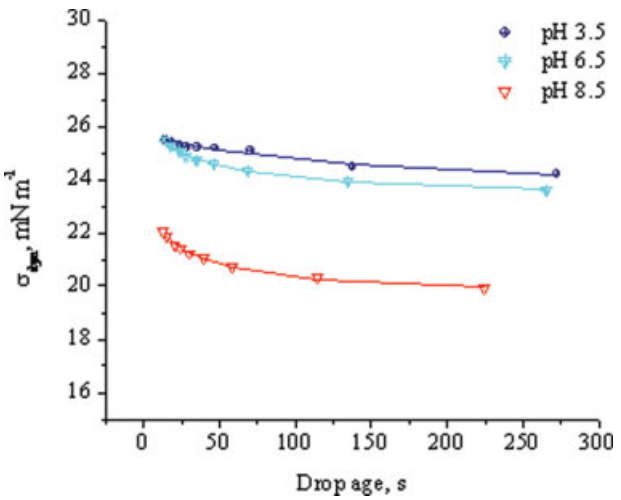

Figure 2. Dynamic interfacial tension of 25 wt % heavy oil-in-toluene with mpH_2O at varied pH, measured by drop volume technique (DVT).

Lines are diffusion-limited model fitted to the data (symbols). [Color figure can be viewed in the online issue, which is available at www.interscience.wiley.com.]

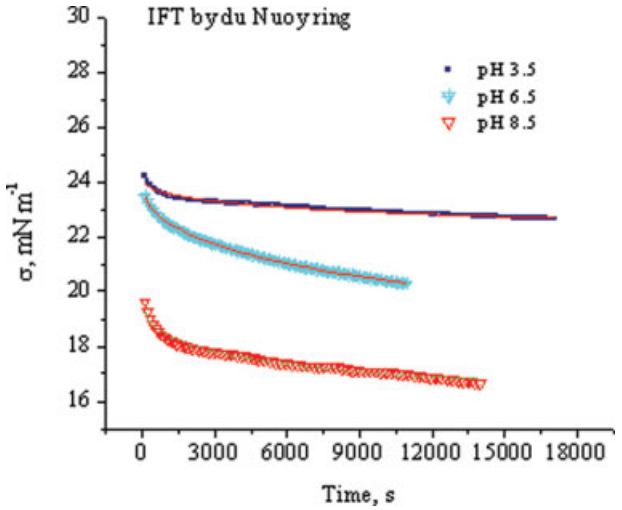

Figure 3. Interfacial tension of 25 wt % heavy oil-in-toluene with mpH_2O at varied pH as measured by du Nuoy ring technique.

Lines are diffusion-limited model fitted to the data (symbols). [Color figure can be viewed in the online issue, which is available at www.interscience.wiley.com.]

for adsorption will indicate a lowered interfacial tension in these cases.

The interfacial tension measurements were repeated using the Du Nuoy ring technique, which is at near static equilibrium conditions, and hence measurements were made for a longer time scale. This allows time for development of full interfacial activity. As pH increased, the order of the curves in Figure 3 remained the same as in Figure 2, but the interfacial tensions were much lower. Prolonged decreases in interfacial tension as a function of time signify either reorganization of interfacially active materials in heavy oil or slow diffusion of surface-active molecules from inside the droplets to the interface. Slow decline of interfacial tension over extended time has been attributed by others to reordering of asphaltenes in studies of dynamic interfacial tensions of crude oils.[15–19]

The implication for slow adsorption at a particular low pH during mixing is that during droplet deformation interfacial stretching would leave bare surface (high interfacial tension) for contact with other drops. Hence coalescence could occur quickly on impact of bare patches when droplets collide before surfactant annealing occurs, and also if repulsive forces between the particles are reduced (shown by smaller negative zeta potentials).

Zeta potential of heavy oil droplets and colloidal sand in mpH_2O as a function of pH

Electrical double layer repulsive and other colloidal forces control interactions between the drops, and between the drops and sand granules in a nondynamic environment. The repulsive forces are modified by pH (which reflects the concentrations of potential determining ions) and by the electrolyte concentrations and/or counterions that cause double layer compression, thus changing the zeta potentials of oil and sand surface/interfaces. Figure 4 shows the zeta potential for

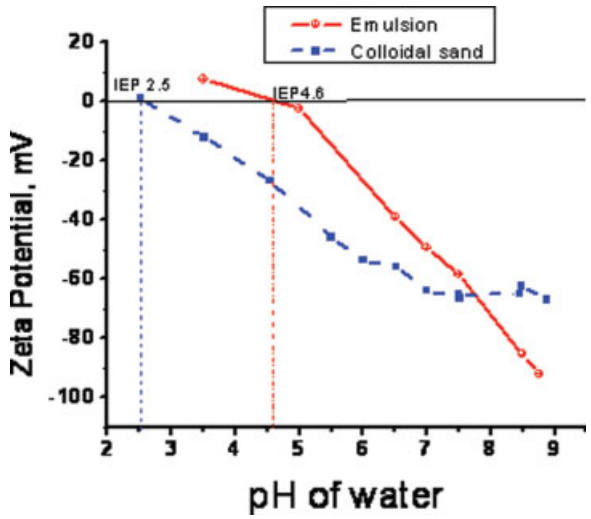

Figure 4. Zeta potential of emulsion droplets and colloidal sand as a function of pH. Lines indicate the isoelectric points.

[Color figure can be viewed in the online issue, which is available at www.interscience.wiley.com.]

the diluted heavy oil droplets and the colloidal quartz particles measured as a function of pH of the process water. Both systems are similarly negatively charged at pH 7.75, and at higher pH the oil droplets show larger negative zeta potential than colloidal quartz. The isoelectric pH for emulsions is 4.6 and the quartz is 2.5. At pH 8.5 and 6.5, both systems are negatively charged and should not coagulate. At pH 4.6, however, conditions for attraction of the particles are achieved through reduction of the zeta potentials to zero for the oil droplets at the isoelectric point. Here quartz particles have an average zeta potential of −27 mV. At pH 3.5 the oil droplets are positively charged (reaction 8) and the quartz particles are still negatively charged (see reactions 4–5) thus approaching conditions for electrostatic attraction between the two types of particles. These effects are manifested in the droplet sizes during turbulent mixing when droplets deform, collide, breakup, and coalesce. The results below are shown at various pH for mixing with and without sand present. Size distributions and microscopy data give the details of the droplet sizes.

For quartz the reactions are

$$SiO_2 + H_2O \rightleftharpoons Si\text{—}O^- + 2OH^- \tag{4}$$

$$Si\text{—}O^- + H_2O \rightleftharpoons Si\text{—}OH + OH^- \tag{5}$$

$$Si\text{—}OH + H_3O^+ \rightleftharpoons Si\text{—}OH_2^+ + H_2O \tag{6}$$

For oil droplet surfaces, the reactions that are possible

$$\equiv RCOO^- + H_3O^+ \rightleftharpoons R\text{—}COOH_s + H_2O \tag{7}$$

$$\equiv R\text{—}NH_2 + H^+Cl^- \rightleftharpoons \equiv R\text{—}NH_3^+ + Cl^- \tag{8}$$

The possibility of amines present will confer positive charges at low pH.

Emulsion droplets sizes as a function of mixing time

Sauter Mean Diameters of Droplets with and Without Sand Present at pH 8.5. Figure 5 shows the decrease in Sauter mean diameter (points) of emulsion droplets plotted as a function of mixing times for two oil volume fractions in the presence (lower curves) and absence (upper curves) of a fixed volume fraction of sand. The steady-state droplet size was previously determined to be a function of time of mixing in an exponential decay or first order rate equation (lines).[1]

$$d_{32} = d_{32}^{ss} + B\exp(-k_1 t) \tag{9}$$

where superscript ss means steady state, B is a constant and k_1 is a rate constant, d is droplet diameter, and t is time. At pH 8.5, mixing an increased fraction of oil (from $\Phi_{oil} = 0.05$ to $\Phi_{oil} = 0.1$) in mpH_2O at 800 rpm, produces higher droplet number-density thus increasing the probability of collision between droplets with mixing time. It was previously shown in our earlier studies that, as oil fraction increased systematically the droplets sizes became larger.[2] The following result is consistent with observed previous findings of increase in droplets size as Φ_{oil} became greater during turbulent mixing.[2,20–22] The droplet sizes plotted against mixing time at the higher volume fraction of diluted heavy oil ($\Phi_{oil} = 0.1$), with and without sand, parallel to the behavior for lower oil fraction $\Phi_{oil} = 0.05$. In the presence of sand, during mixing with increased oil fraction at pH 8.5 (Figure 5), the droplets are close in size as oil fraction increased. We have shown in previous studies that at pH 8.5, for one oil fraction $\Phi_{oil} = 0.05$ mixed with sand at 800 rpm, the steady-state droplet size was a function of sand fraction.[1]

Sauter Mean Diameters of Droplets with and Without Sand Present at pH 6.5. Figure 6 shows two effects of turbulent mixing of oils at volume fractions of 0.05 and 0.1 as a function of mixing time at pH 6.5 in mpH_2O in the presence and absence of sand. The first effect was that at pH 6.5

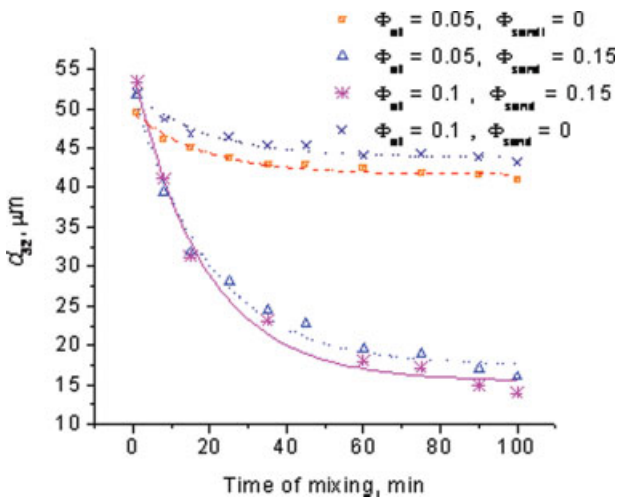

Figure 5. Droplet diameter vs. mixing time at 800 rpm; two volume fractions 0.05, 0.1 of 25 wt % heavy oil diluted in toluene, in model process water at pH 8.5 with and without sand.[1]

Lines are the fitted function for Eq. 9. [Color figure can be viewed in the online issue, which is available at www.interscience.wiley.com.]

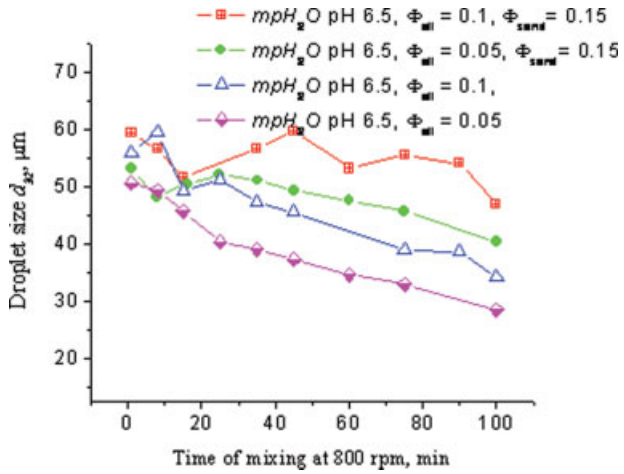

Figure 6. Changes in Sauter mean diameters of oil droplets during mixing at 800 rpm in the presence and absence of sand in mpH$_2$O at pH 6.5.

[Color figure can be viewed in the online issue, which is available at www.interscience.wiley.com.]

droplet size-time curves for $\Phi_{oil} = 0.1$ were always above that for $\Phi_{oil} = 0.05$, both for the presence and absence of sand. The second effect was that mixing with sand at pH 6.5 caused formation of droplets that were larger than those without sand. This meant that increased coalescence and/or reduced breakage occurred. This was opposite to the results at pH 8.5 where mixing with sand at pH 8.5 caused the formation of smaller droplets than without sand (Figure 5). The effect will also be shown later in more detail under the topic of droplet size distributions.

Sauter Mean Diameters of Droplets at pH 3.5 Compared with pH 6.5 and 8.5. When heavy oil was mixed in mpH$_2$O at pH 3.5 without sand, the emulsion was very unstable and the average droplet size fluctuated with mixing time. Figure 7 compares the droplet sizes for the same oil fraction of 0.1 mixed in mpH$_2$O at pH 3.5 with the droplet sizes at pH 6.5 and 8.5. The top curve of Figure 7 shows the fluctuation of

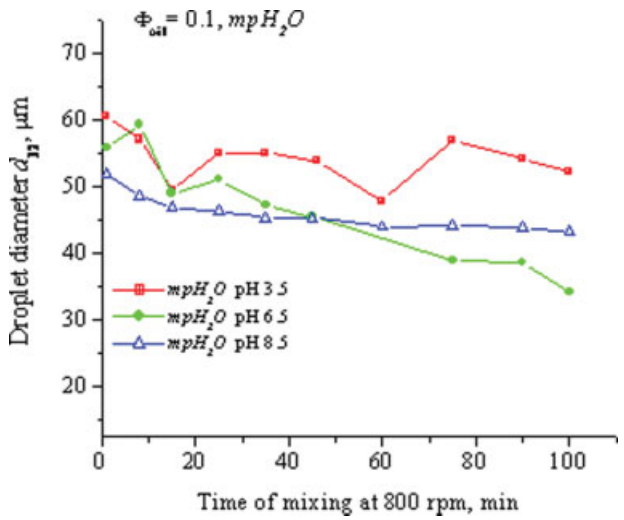

Figure 7. Dynamic changes in droplet size with time of mixing at 800 rpm for $\Phi_{oil} = 0.1$ in mpH$_2$O pH 3.5, 6.5, and 8.5.

[Color figure can be viewed in the online issue, which is available at www.interscience.wiley.com.]

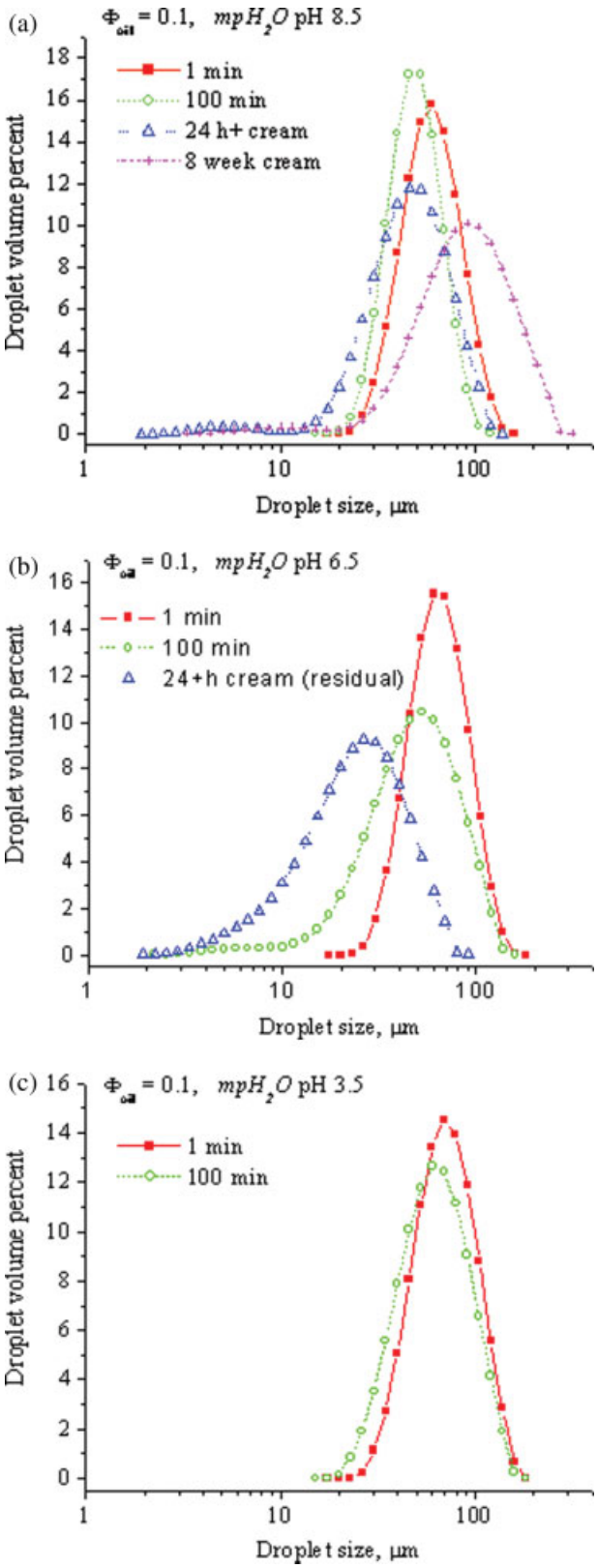

Table 3. Size Data for Emulsions Described in Figures 8a–c

Size Distribution	1 min Sizes, μm (red)	100 min Sizes, μm (green)	Rest 24 h + sizes, μm (blue)	Water − mpH_2O pH
a d_{10} – d_{90}	35.6–84.5	30.6–66.6	22.6–73.8	8.5
d_{32}, span	52.0, 0.89	43.2, 0.79	33.1, 1.19	
a* d_{10} – d_{90}			*39.9–158.3	
d_{32}, span			62.5, 1.77	8.5
b d_{10} – d_{90}	38.3–91.0	21.0–82.2	8.91–43.9	
d_{32}, span	55.6, 0.89	34.2, 1.36	16.8, 1.56	6.5
c d_{10} – d_{90}	40.5–102.9	33.2–96.3	No droplets left	
d_{32}, span	60.8, 0.96	52.4, 1.11		3.5

*Eight weeks later.

d_{32} vs. time at pH 3.5. Drop sizes are generally larger than those at pH 6.5 and pH 8.5 in mpH_2O. For turbulent mixing of the same oil fraction of 0.1 at pH 6.5, after 45 min the droplets sizes decreased more than droplets sizes formed for pH 8.5 and pH 3.5.

In the presence of sand at pH 3.5, the Sauter mean diameters of droplets could not be measured easily because most of the oil coalesced and remained within the sand bed. The droplets micrographs in the absence of sand and in the presence of sand are shown in the sections to follow. The size distributions in the presence of sand are also shown later.

Size distributions of droplets at pH 8.5, 6.5, and 3.5 in the absence of sand

Droplet size distributions are shown in Figures 8a–c. Size distributions after 1 min and 100 min of mixing and 24 h after rest are compared at each pH. At pH 8.5, the size distributions of droplets were also measured 1–8 weeks after mixing ceased. It was observed that, even at pH 8.5 in a buffered system, coalescence occurred slowly over weeks, even though it was not apparent after 24 h. After the long rest time, coalescence was evidenced in droplet sizes larger than their sizes for the initial 1- and 100-min mixing durations (see Table 3), shown in a broadened lognormal distribution and in the span, where the span is the dimensionless description of the size distribution width ($d_{90} - d_{10}$)divided by d_{50}. The absence of droplets indicated separation of the oil phase from the water phase.

The size distributions in Figure 8c show a small change in sizes of droplets between 1 and 100 min of mixing. It appears from the size distributions that finer droplets were produced as mixing times increased, but their lifetimes were short. After 24 h at pH 3.5, all the droplets coalesced into the free oil layer and sizes could not be measured. After sampling the emulsions during the mixing and quickly observing them by microscopy, the large droplets were seen to be assimilating the finer droplets within a few seconds.

Micrographs of oil droplets in water in the absence of sand at pH 3.5

The micrographs produced over various mixing times for these systems are shown in Figures 9a–e. At pH 3.5, the droplets also formed multiple O/W/O emulsions throughout the mixing times. The appearance of multiple emulsions in Figures 9a, b, d, e indicated that inversion was occurring. At this pH, flocculated stringy materials seen in micrograph (e) came from the oil. These readily broke into free oil when attempts were made to remove them. The micrograph (e) shows that the emulsions were gathered together by this stringy material. The fluctuations in measured averaged sizes (Figure 7) and the shift toward larger size distributions of the

Figure 8. Droplet size distributions for Φ_{oil} = 0.1 in mpH_2O, where the lines are lognormal distribution fit.

(a) pH 8.5, showing breakage after mixing for 1 min and 100 min, and coalescence after 24 h and 8 weeks rest. (b) pH 6.5, after mixing for 1min, 100 min, and 24 h rest, most large droplets that coalesced to free oil were not measured. (c) pH 3.5, after mixing for 1 min and 100 min. After 24 h, in this case there were no droplets left. [Color figure can be viewed in the online issue, which is available at www.interscience.wiley.com.]

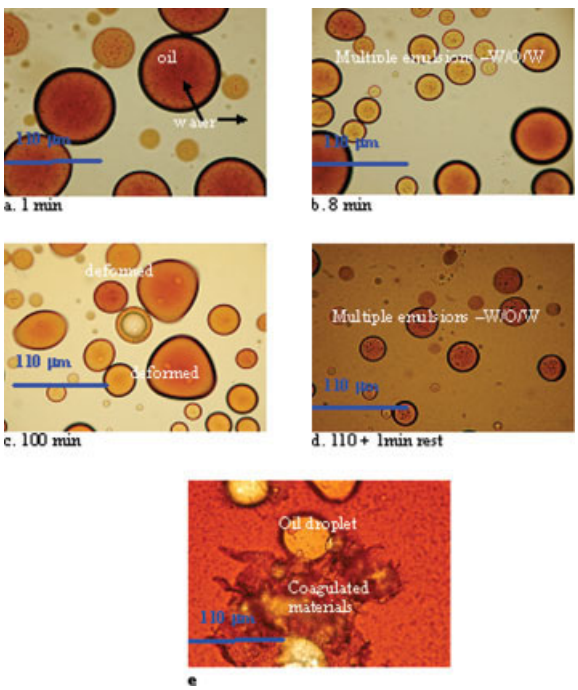

Figure 9. Micrographs (a–e) of Φ_{oil} = 0.1 mixed in mpH_2O, pH 3.5, no sand, 800 rpm.

Multiple O/W/O emulsions are shown in all of the samples. [Color figure can be viewed in the online issue, which is available at www.interscience.wiley.com.]

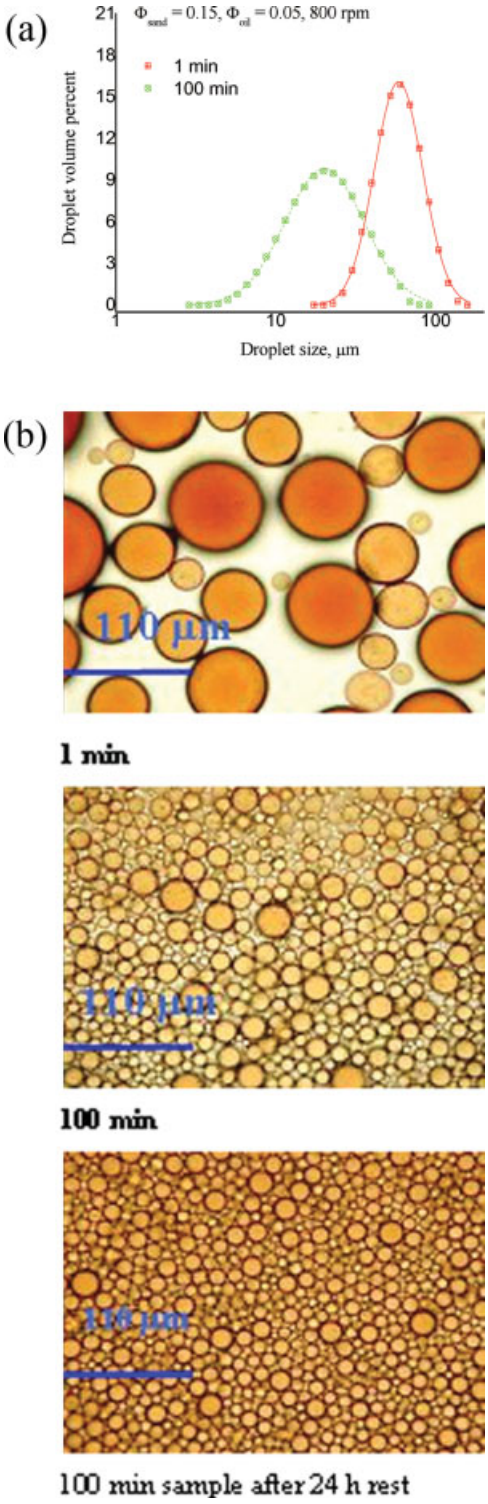

Figure 10. (a) Droplet size distributions of emulsions after mixing diluted heavy oil (Φ = 0.05) with sand at 800 rpm in mpH_2O at pH 8.5 for 1 min and 100 min. (b) Micrographs of emulsions after mixing diluted heavy oil (Φ = 0.05) with sand at 800 rpm in mpH_2O at pH 8.5 for 1 min, 100 min and after 100 min sample was allowed to rest for 24 h.

[Color figure can be viewed in the online issue, which is available at www.interscience.wiley.com.]

measurable emulsions at pH 3.5 (Figure 8c) are consistent with these micrographs.

Size distributions of oil droplets at pH 3.5, 6.5, and pH 8.5 in the presence of sand

The size distributions of emulsions produced after mixing diluted heavy oil in the mpH_2O at pH 8.5 with sand are presented in Figure 10a as a reference for comparing observed changes when pH was reduced. Figure 10a shows the emulsion droplet size distributions after 1 min and 100 min of mixing. The corresponding micrographs for the samples in Figure 10b show fine emulsions after 1 min and 100 min mixing, and the stable fine droplets of the 100 min sample after 24 h rest. The scales are embedded.

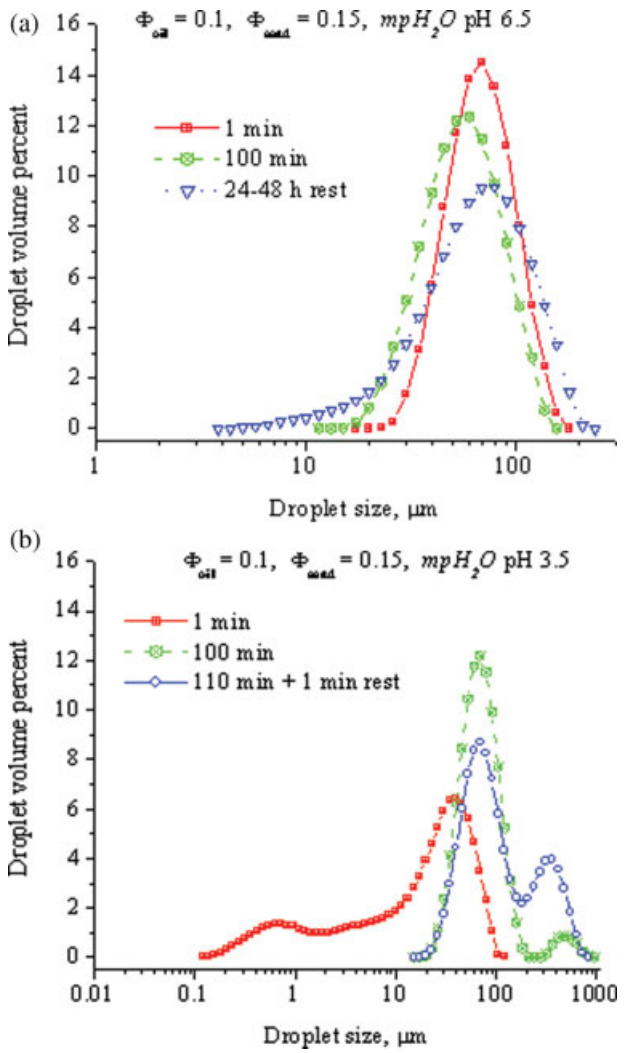

Figure 11. Droplet size distributions after 1 min and 100 min of mixing Φ_{oil} = 0.1 in mpH_2O.

(a) pH 6.5, with sand at 800 rpm. Droplet coalescence after 24–48 h rest is shown by the shift to larger droplets. (b) pH 3.5, with sand showing droplets breakage after 1 min, coalescence after 100 min, and after 110 min mixing with 1 min rest. [Color figure can be viewed in the online issue, which is available at www.interscience.wiley.com.]

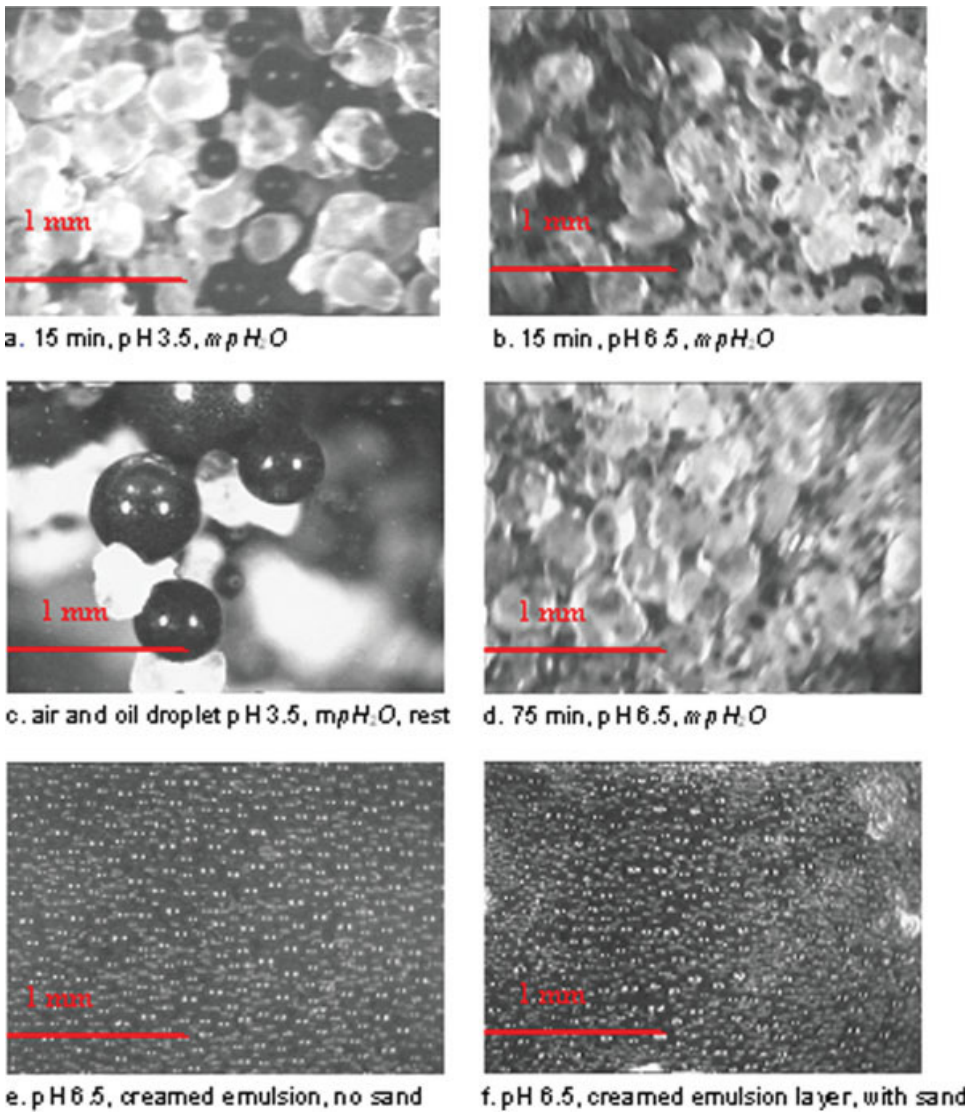

Figure 12. Videomicrographs of oil droplets (Φ_{oil} = 0.1) in sand and mpH_2O, pH 3.5 and 6.5 during and after mixing at 800 rpm in mixing tank.

[Color figure can be viewed in the online issue, which is available at www.interscience.wiley.com.]

The droplet size distributions at pH 6.5 formed after 1 and 100 min of turbulent mixing at 800 rpm with sand in mpH_2O and after 24–48 h rest are shown in Figure 11a. Coalescence after 24 h of rest was very apparent for the systems with sand at pH 6.5. The size distributions appear to tail off into a broader distribution of finer droplets because the coarser droplets creamed and coalesced into free oil and could not be measured. Previously, Figures 8a–c showed the droplet size distributions without sand for Φ_{oil} = 0.1 and it appeared that the creamed samples contained more fine than coarse droplets as well. The coarse drops coalesced into a free oil phase after 24 h as well.

Figure 11b shows the droplet sizes from mixing oil with sand and water at pH 3.5. The observations were that the droplets were very unstable even in sampling and resulted in larger droplets and wide distributions. Previously, under two-phase mixing, Figure 8c showed the mixing results at pH 3.5 in mpH_2O for a Φ_{oil} = 0.1 as compared with the results at pH 6.5 and 8.5 (see Figures 8a, b). The largest average droplet sizes were measured for pH 3.5. A decrease of pH from 6.5 to 3.5 allows more available H^+ ions for interaction with the oil/water interface. H^+ ions are potential-determining and, by chemical interaction with surface groups, whether they are oxides, amines, or carboxylates, protonation changes the negative zeta potential toward more positive values. This was discussed for the oil/water and the sand/water interfaces in the previous section on zeta potential. Reduced repulsive forces between particles affect sand–water–oil interactions and eventually, the sizes of droplets become larger from coalescence as their stability is reduced.

In Figure 11a for pH 6.5 with sand at the same heavy oil volume fraction, the droplet size distributions appeared to be almost the same as that at pH 3.5 without sand as in Figure 8c shown previously. At lowered pH and in the presence of sand,

the O/W emulsions were the least stable. In the presence of sand, the oil droplets at pH 3.5 were much larger than the droplets in the absence of sand and the droplets were trapped between the sand grains by electrostatic attraction.

Mixing heavy oil in mpH_2O at pH 3.5 with sand produced immediate entrapment and some heterocoagulation (see video images below). Even at high kinetic energy in mixing, most of the oil droplets remained trapped in the sand bed, and extraction of droplets to water phase was difficult. The water phase remained very clear even after 100 min of mixing at 800 rpm. Figure 11b shows the size distributions of oil droplets that were released by gently tapping the tank then pouring out after 1 min rest. The micrographs and the video-micrographs as well indicated multi-modal size distributions of unstable oil droplets. These were unlike the distribution without sand shown in Figure 8c previously. The sand-enhanced coalescence produced various sizes of droplets. The extremely large sizes may be coagulated materials from oil (shown previously in Figure 9) and colloidal materials from dissolved sand agglomerated with oils when mixed together with the oil droplets, which were released from the sand bed.

Three-Phase Emulsification Video Images in mpH_2O at Different pH. Figure 12 shows the video-micrograph of heavy oil droplets and sand captured during mixing and after settling at pH 3.5 and at pH 6.5. The oil droplets remained large at pH 6.5 and 3.5 throughout mixing with sand. At pH 3.5, the size distributions of the oil droplets vs. time of mixing were difficult to follow by either microscopy or light scattering because the oil droplets were held between the sand grains creating a fluffy appearance of the deposit. Oil was seen as black spots. The sand and oil remained associated indefinitely if undisturbed. However, if the mixture was poured out of the tank into jars, some of the oil was released from the sand and free oil floated to the top of the vessel. No droplets were seen in this top phase. The sand, oil, and water together were removed with a spoon for observation on a microscope slide. However, by removal and placing on the slide, the droplets broke revealing free oil flowing between the sand grains, but not adhering to the sand.

Figure 12 also shows the video-recorded captured creamed emulsions for pH 6.5 without sand. Creamed droplets that were formed without sand (image e) were uniformly packed as compared with the random packing of those formed with sand (image f). For pH 6.5 droplets, with sand, there was entrapment of the oil within the sand and these were similar to droplets in mpH_2O pH 3.5 with sand. Drop–drop coalescence was enhanced during flow of oil droplets through the bed of sand which caused deformation of the droplets.

We also observed that the oil mixed with sand in unbuffered systems (no bicarbonate, either NaCl or deionized water) formed large droplets that were instantly coalesced and were trapped in sand. This indicated that surface active functional groups were not adsorbed or developed at the interface. Such systems were immediately unstable. Sand acted as a coalescer immediately. Size distribution data could not be collected for these systems.

Conclusions

(1) Equal volume fractions of heavy oil turbulently mixed for 100 min at various pH and buffered model process waters produce droplets sizes in the following order: d_{32} at pH 3.5 (mpH_2O) > d_{32} at pH 6.5 (mpH_2O) > d_{32} at pH 8.5 (mpH_2O). The oil/water interfacial tensions as a function of time was largest at pH 3.5 > pH 6.5 > pH 8.5.

(2) Zeta potentials of oil droplets were highly negative in all buffered waters at pH > 8.5. Zeta potentials of droplets decreased as pH decreased, reaching an isoelectric point around of 4.6 in the absence of sand. Droplets were positively charged at pH 3.5. Positively charged droplets of oil at pH 3.5, also formed O/W/O emulsions.

(3) Sand was still negatively charged at pH 3.5. Electrostatic attraction between sand and oil at low pH promoted coalescence during mixing.

(4) In the presence of sand, the surface properties of both the sand and oil contributed to the final droplet sizes in turbulent flow. Droplet breakage was enhanced by sand at high pH 8.5 in bicarbonate buffered mpH_2O. Droplet coalescence was enhanced by sand at pH 6.5 and 3.5 in bicarbonate buffered mpH_2O water.

(5) Droplets in unbuffered systems (no bicarbonate, either NaCl or deionized water) with sand were instantly coalesced and trapped in sand. Such systems were immediately unstable. Sand acted as a coalescer.

Acknowledgments

Part of this work was supported by the Government of Canada Panel of Energy Research and Development. The technical assistance of Ms. Ngo is appreciated.

Notation

A = Hamaker constant
a = the particle radius, m
H = the interparticle separation, m
B = coefficient
b_{bl} = blade length, cm
Con. = constant
c = continuous phase
D_T = tank diameter cm
D = impeller diameter, cm
d_{32} = Sauter mean diameter, μm $d_{32} = \frac{\sum_i^k n_i d_i^3}{\sum_i^k n_i d_i^2}$
d_{32}^* = momentary Sauter mean diameter, μm
d_{32}^{SS} = Sauter mean diameter at steady state (ss), μm
d_{10} = diameter, i.e.,10% of the population is less than its value, μm
d_{50} = median diameter, i.e., 50% of the population is less than its value, μm
d_{90} = diameter where 90% of the population is less than its value, μm
H = liquid height, cm
k_1 = kinetic rate constant, min^{-1}
IEP = isoelectric point
IFT = interfacial tension
mpH_2O = model process water
N = rotational speed, rev/s
PTFE = polytetrafluoroethylene or teflon
R^2 = variance
Re = Reynolds number $Re = \frac{ND^2\rho_c}{\eta_c}$
rpm = revolutions per minute
rps = revolutions per second
span = $(d_{90}\text{-}d_{10})/d_{50}$
t = time, min
V = impeller tip velocity = 0.16 rps
w = blade width, cm
W = watts
We = Weber number = $\frac{\rho_c D^3 N^2}{\sigma}$
V_T = total potential energy is the sum of competing contributions from

V_A = attractive forces
V_R = repulsive forces
V_S = hydration forces from water

Greek letters

ε_T = energy dissipation per unit mass (W/kg = m^2/s^3) in the tank
κ = the inverse electrical double layer thickness dependent on the ionic strength
Φ_{oil} = volume fraction of 25 wt % heavy oil diluted in toluene
Φ_{sand} = volume fraction of sand
ρ_c = density of continuous phase, kg/m^3
η_c = viscosity of continuous phase, (s kg)/m^2
σ = equilibrium interfacial tension, mN/m^1
ζ = the zeta potential, mV

Literature Cited

1. Angle CW. Effects of sand fraction on toluene-diluted heavy oil in water emulsions in turbulent flow. *Can J Chem Eng*. 2004;82:722–734.
2. Angle CW, Hamza HA. Drop sizes during turbulent mixing of toluene-heavy oil fractions in water. *AIChE J*. 2006;52:2639–2650.
3. Angle CW, Dabros T, Hamza HA. Predicting sizes of toluene-diluted heavy oil emulsions in turbulent flow, Part 1: application of two adsorption kinetic models for σ^E in two size predictive models. *Chem. Eng. Sci*. 2006;61:7309–7324.
4. Angle CW, Hamza HA. Predicting the sizes of toluene-diluted heavy oil emulsions in turbulent flow, Part 2: Hinze-Kolmogorov based model adapted for increased oil fractions and energy dissipation in a stirred tank. *Chem Eng Sci*. 2006;61:7325–7335.
5. Angle CW, Dabros T, Hamza HA. Demulsifier effectiveness in treating heavy oil emulsions in the presence of fine sands in the production fluids. *Energy Fuels*. 2007;21:912–919.
6. Angle CW, Hamza HA, Dabros T. Size distributions and stability of toluene diluted heavy oil emulsions. *AIChE J*. 2006;52:1257–1266.
7. Angle CW, Long Y, Hamza HA, Lue L. Precipitation of asphaltenes from solvent-diluted heavy oil and thermodynamic properties of solvent-diluted heavy oil solutions. *Fuel*. 2006;85:492–506.
8. Bulmer JT, Star J. *Syncrude Analytical Methods for Oil Sand and Bitumen Processing*. Edmonton: The Alberta Oil Sands Technology and Research Authority, 1979.
9. Hunter RJ. *Zeta Potential in Colloid Science—Principles and Application*. New York: Academic Press, 1981.
10. Krüss U. Standard test methods for interfacial tension of oil against water by the ring method. Technical information on Krüss Tensiometers ASTM D[0971–91]. Palo Alto CA: Kruss 2008.
11. Angle C. Stability of Heavy Oil Emulsions in Turbulent Flow and Different Chemical Environments. 1-424. PhD Diss. University of Manchester Institute of Science and Technology, Manchester, UK.
12. Kolmogorov AM. Breakup of droplets in turbulent flow. *Dokl Acad Nauk USSR*. 1949;66:825–828.
13. Hinze JO. Fundamentals of the hydrodynamic mechanisms of splitting in dispersion processes. *AIChE J*. 1955;1:289–295.
14. Hunter RJ. Thin films: emulsions. Foundations in Colloid Science, vol. II Ch. 15 (thin films), Ch16 (emulsions). Oxford: Clarendon Press, New York, 1989.
15. Bonfillon A, Langevin D. Viscoelasticity of monolayers at the oil-water interface. *Langmuir*. 1993;9:2172–2177.
16. Sheu EY, DeTar MM, Storm DA. Interfacial properties of asphaltenes. *Fuel*. 1992;71:1277–1281.
17. Sheu EY, Shields MB. Asphaltene surface activity at oil/water interfaces. SPE. SPE 28995. In International Symposium on Oilfield Chemistry, San Antonio Texas, 1995:523–532.
18. Sheu EY, Storm DA, Shields MB. Adsorption kinetics of asphaltenes at toluene/acid solution interface. *Fuel*. 1995;74:1475–1479.
19. Bauget F, Langevin D, Lenormand R. Dynamic surface properties of asphaltenes and resins at the oil-air interface. *J Colloid Interface Sci*. 2001;239:501–508.
20. Chatzi EG, Kiparissides C. Steady-state drop-size distributions in high holdup fraction dispersion systems. *AIChE J*. 1995;41:1640–1652.
21. Doulah MS. An effect of hold-up on drop sizes in liquid-liquid dispersions. *Ind Eng Chem Fundam.* 1975;14:137–138.
22. Desnoyer C, Masbernat O, Gourdon C. Experimental study of drop size distributions at high phase ratio in liquid-liquid dispersions. *Chem Eng Sci*. 2003;58:1353–1363.

Manuscript received Nov. 8, 2007, and revision received Aug. 1, 2008.